Journal of Photochemistry & Photobiology, B: Biology 278 (2026) 113429

Contents lists available at ScienceDirect

Journal of Photochemistry & Photobiology, B: Biology

journal homepage: www.elsevier.com/locate/jphotobiol

Subcellular photoprotection through precision nutraceuticals: Divergent actions of rutin and punicalagin on redox and mitochondrial homeostasis in human dermal fibroblasts

Alessia Riente [a,b,*], Flavio Di Giacinto [a,c,*], Michele Maria De Giulio [a,b], Benedetta Niccolini [d], Elisabetta Tabolacci [d,e], Maria Elisabetta Clementi [f], Marco De Spirito [a,b], Giuseppe Maulucci [a,b,*]

[a] Dipartimento di Neuroscienze, Metabolic Intelligence Lab, Università Cattolica del Sacro Cuore, Largo Francesco Vito, 1, 00168 Rome, Italy
[b] UOC Fisica per le Scienze della Vita, Fondazione Policlinico Universitario "A. Gemelli" IRCCS, 00168 Rome, Italy
[c] Department of Life Science, Health, and Health Professions, Link Campus University, Via del Casale di S. Pio V, 44, 00165 Rome, Italy
[d] UOC Genetica Medica, Fondazione Policlinico Universitario A. Gemelli IRCCS, 00168 Rome, Italy
[e] Dipartimento di Scienze della Vita e Sanità Pubblica, Sezione di Medicina Genomica, Università Cattolica del Sacro Cuore, Largo F. Vito 1, 00168 Rome, Italy
[f] Istituto di Scienze e Tecnologie Chimiche "Giulio Natta" SCITEC-CNR, Largo Francesco Vito 1, 00168 Rome, Italy,

ARTICLE INFO

Keywords:
Polyphenols
UVA photoprotection
Oxidative stress
Fluorescence lifetime imaging microscopy
Phasor analysis

ABSTRACT

Excessive ultraviolet A (UVA) exposure is a major environmental factor contributing to skin photoaging and oxidative damage. Identifying natural compounds that can counteract these effects is increasingly relevant for preventive and personalized healthcare. Precision nutrition uses diet-derived bioactives to modulate molecular pathways in defined cellular contexts. Polyphenols are promising for sustaining redox and metabolic balance under stress. This study examined the photoprotective actions of rutin (buckwheat, citrus peel) and punicalagin (pomegranate) in human dermal fibroblasts exposed to UVA radiation. Phasor-based fluorescence lifetime imaging microscopy (FLIM) quantified lipid peroxidation–related oxidative stress (F_{ox}) and oxidative phosphorylation activity (F_{oxphos}). Mitochondrial morphology was assessed via fission (Fis1) and fusion (MFN2) markers. Though UVA exposure tended to increase oxidative stress, the observed variation is not significant. Rutin provided superior antioxidant protection under UVA stress, substantially reducing F_{ox} to 0.129 ± 0.02 with a near-significant trend, while punicalagin demonstrated stronger baseline antioxidant activity. Both compounds enhanced oxidative phosphorylation under stress: punicalagin increased F_{oxphos} to 0.823 ± 0.02 ($p = 0.004$ vs UVA) and rutin to 0.789 ± 0.02 ($p = 0.023$ vs UVA). UVA disrupted mitochondrial networks, elevating fission and reducing fusion. Rutin reversed these effects, restoring fusion and reducing fission, whereas punicalagin provided partial recovery. In summary, rutin offered broader cytoprotection by mitigating oxidative stress and preserving mitochondrial integrity, while punicalagin mainly supported metabolic activity. These distinct responses highlight polyphenol-based nutraceuticals as precision tools for targeted skin photoprotection, suggesting their potential use in dietary or topical formulations to counteract everyday UVA exposure and photoaging.

1. Introduction

Ultraviolet (UV) radiation is a major environmental factor with both beneficial and harmful health effects. While controlled exposure is essential for vitamin D synthesis and circadian rhythm regulation, excessive exposure is a major risk factor for skin damage and carcinogenesis [1]. UV radiation is classified by wavelength into UVA (315–400 nm) and UVB (280–315 nm). UVA, which constitutes about 95% of the

* Corresponding authors at: Dipartimento di Neuroscienze, Metabolic Intelligence Lab, Università Cattolica del Sacro Cuore, Largo Francesco Vito, 1, 00168 Rome, Italy.
E-mail addresses: alessia.riente@unicatt.it (A. Riente), flavio.digiancinto@unicatt.it (F. Di Giacinto), michelemaria.degiulio@unicatt.it (M.M. De Giulio), elisabetta.tabolacci@unicatt.it (E. Tabolacci), elisabetta.clementi@scitec.cnr.it (M.E. Clementi), marco.despirito@unicatt.it (M. De Spirito), giuseppe.maulucci@unicatt.it (G. Maulucci).

https://doi.org/10.1016/j.jphotobiol.2026.113429
Received 3 September 2025; Received in revised form 13 March 2026; Accepted 16 March 2026
Available online 21 March 2026
1011-1344/© 2026 The Authors. Published by Elsevier B.V. This is an open access article under the CC BY-NC-ND license (http://creativecommons.org/licenses/by-nc-nd/4.0/).

UV radiation reaching the Earth's surface, penetrates more deeply into the skin compared to UVB, which primarily affects the epidermis and causes direct DNA damage [2,3]. Unlike UVB, UVA does not directly alter DNA but induces oxidative stress through the generation of reactive oxygen species (ROS). These ROS interact with cellular lipids, proteins, and DNA, causing structural and functional impairments [4,5]. Over time, UVA exposure contributes to photoaging and increases the risk of melanoma, basal cell carcinoma, and squamous cell carcinoma [6,7]. In dermal fibroblasts, which are directly targeted due to UVA's deeper penetration, chronic UVA exposure leads to mitochondrial dysfunction, extracellular matrix (ECM) degradation, and apoptosis. This process impairs the synthesis of key ECM proteins, accelerating skin aging and compromising tissue integrity [4,8–10]. The accumulation of ROS is now recognized as a central mechanism in photodamage, photoaging, and photocarcinogenesis [11–14]. Understanding these molecular pathways is critical for developing effective photoprotective strategies [3]. Natural bioactive compounds are increasingly studied for their ability to counteract oxidative stress, both as nutraceuticals and in topical applications. Nutraceuticals are defined as compounds derived from food that offer health benefits beyond basic nutrition. They are a promising addition to, or alternative for, conventional pharmaceutical and dermatological approaches. Among these, polyphenols are particularly noteworthy due to their antioxidant and anti- inflammatory properties, which contribute to the prevention of chronic diseases such as cancer, diabetes, and cardiovascular disorders [15]. Among them, punicalagin and rutin deserve particular attention for the effects, standing out for their cytoprotective properties, especially in the context of UVA-induced oxidative stress [16,17]. In recent years, several studies have expanded the understanding of polyphenol-based nutraceuticals beyond classical antioxidant activity, highlighting their capacity to modulate stress-responsive pathways and cellular metabolism in multiple biological models [18–20]. Rutin, for instance, has been shown to mitigate oxidative and inflammatory responses in rodents and Drosophila exposed to high-sucrose diets or chemical stressors, improving mitochondrial performance and lipid homeostasis [18,21]. Similarly, punicalagin has demonstrated protective effects against reproductive and hepatic toxicity induced by heavy metals or xenobiotics, mainly through the activation of Nrf2, SIRT1, and mitochondrial biogenesis pathways [22]. These findings indicate that both compounds exert pleiotropic regulatory actions on redox-sensitive signaling networks and energy metabolism, supporting their potential role as systemic modulators of cellular resilience. Integrating these insights with skin-targeted studies suggests that rutin and punicalagin could act as prototype precision nutraceuticals capable of buffering oxidative challenges not only in dermal fibroblasts but also in diverse metabolic and stress-related contexts. Rutin, a flavonoid found in foods such as buckwheat, apricots, cherries, grapefruit, plums, and oranges, is also abundant in grape by-products from wine production [23–25]. Punicalagin, a polyphenol extracted from pomegranate, is recognized for its strong antioxidant capacity [26]. These compounds demonstrate how nutraceuticals can be used to protect the skin systemically or locally, by reinforcing cellular antioxidant defences and supporting mitochondrial health under oxidative stress. This study aims to elucidate the protective mechanisms of rutin and punicalagin against UVA-induced oxidative stress and metabolic alterations at both cellular and subcellular levels. While the detrimental impact of UVA radiation on skin cells is well established, the intracellular responses, including compartment- specific metabolic shifts and oxidative stress distribution, remain incompletely understood. Oxidative damage to mitochondria disrupts energy metabolism and compromises cellular function [27], while stress-induced DNA damage threatens genomic stability [28]. At the same time, the cytoplasmic environment, which regulates redox balance, plays a key role in the cell's defence against oxidative stress [29]. To address this issue, we used fluorescence lifetime microscopy (FLIM) together with a custom- developed phasor algorithm to simultaneously quantify oxidative stress fractions and metabolic shifts between glycolysis and oxidative phosphorylation inside cells. This methodological approach allows an assessment of UVA-induced damage and elucidates the protective mechanisms of rutin and punicalagins at the subcellular level. By analysing oxidative stress levels and metabolic rebalancing in these compartments, we aim to clarify the efficacy of these polyphenols in attenuating UVA-induced oxidative damage and preserving oxidative phosphorylation. Understanding how specific polyphenols affect photoaging-related pathways at the subcellular level provides a mechanistic basis for their use in personalized nutritional and dermatological strategies. Their inclusion in functional foods or topical formulations align with current trends in precision nutrition, which seeks to tailor nutritional interventions based on molecular, cellular, and individual variability. In this framework, the skin represents a relevant and accessible model to investigate how diet-derived compounds can act as modulators of stress response and metabolic function.

1.1. Objectives of the study

The present study aimed to elucidate the protective mechanisms of the polyphenols rutin and punicalagin against UVA-induced oxidative and metabolic stress in human dermal fibroblasts, thereby broadening current understanding of the biological potential of less commonly investigated dietary polyphenols. Specifically, we sought to:

(i) quantify UVA-induced oxidative stress and metabolic alterations at the subcellular level using phasor-based FLIM;
(ii) assess the effects of rutin and punicalagin on oxidative stress localization and mitochondrial fusion/fission dynamics; and.
(iii) identify complementary mechanisms by which these compounds preserve redox and metabolic homeostasis.

This work provides a mechanistic framework for the potential use of these polyphenols as precision nutraceuticals for skin photoprotection.

2. Materials and methods

2.1. Materials

Dulbecco's Modified Eagle Medium (DMEM) was purchased from Sigma-Aldrich (St. Louis, MO, USA), and phosphate-buffered saline (PBS) from Biowest (France). L-glutamine, penicillin/streptomycin, and fetal bovine serum (FBS) were also obtained from Biowest. Dimethyl sulfoxide (DMSO) was obtained from Avantor® (ScienceCentral). Punicalagin (P0023) and Rutin were purchased from Sigma-Aldrich (St. Louis, MO, USA). The chemical structures of rutin and punicalagin are shown in Fig. 1. ELISA kits for Fis1 (cat. MBS453299) and Mitofusin-2 (MFN2, cat. MBS2024886) were obtained from MyBiosource Inc. (San Diego, CA, USA). MTS assay kit was acquired by Promega Srl (Padua, Italy). The JC-9 dye (3,3′-dimethyl-α-naftoxacarboxycyanine iodide; cod. D22421) was purchased from Invitrogen (Carlsbad, CA, USA).

2.2. Cells and treatments

Fibroblasts used in the experiments were obtained from a 31-year-old healthy male control (CTRL, coded CTRL1). A 4 mm punch biopsy was performed to collect the skin biopsy, and a primary fibroblast culture was established approximately one week after tissue collection. Informed consent was obtained prior to the skin biopsy, which was performed on the left leg, approximately 10 cm from the ankle (prot. N. 9917/15 and prot. cm 10/15 of the Ethics Committee of the Catholic University of Rome). The cell culture of fibroblasts was grown in DMEM media (Sigma Aldrich, St. Louis, MO, USA) supplemented with 2.5% L-glutamine, 1% penicillin/streptomycin and 10% fetal bovine serum (FBS) (complete medium, CM) at 37 °C with 5% CO_2. Cells at passage number 3 (P3) were plated at 80% confluence for subsequent studies. Each experimental condition was performed in three independent

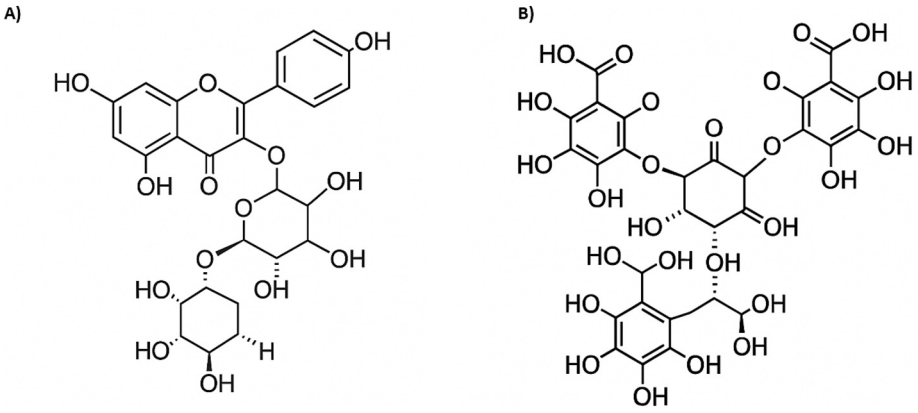

Fig. 1. Chemical structures of the investigated polyphenols. (A) Rutin (quercetin-3-O-rutinoside), a flavonol glycoside widely distributed in fruits and vegetables. (B) Punicalagin, an ellagitannin abundant in pomegranate peel and known for its strong antioxidant activity.

biological experiments, with up to eight technical replicates per condition. A lamp (Vilber Lourmat VL-62C Power 6 W; Vilber Lourmat Deutschland GmbH, Eberhardzell, Germany) set at 365 nm and 10 cm from the source provided UVA dose of approximately 0.432 J/cm^2 This intensity was selected based on previous studies [16,17,30].

This experimental setup is intended to model an acute oxidative stress condition, rather than to reproduce physiological sunlight exposure. During irradiation cells were maintained in PBS without plastic lid in order to minimize radiation absorption by the medium. Immediately after exposure, PBS was replaced with CM, and the cells were left in an incubator for another 24 h before being subjected to various assays. Under the same experimental conditions, non-exposed cells were kept alive for the same period of time. Based on the cell viability results and our previous studies (18,19) we designed the next experiments in which the cells were exposed to UVA radiation for 2 h at an irradiance of 0.06 mJ·cm^{-2}·s^{-1}, resulting in a total delivered dose of 0.432 J/cm^2, using punicalagin and rutin at 10 μM of final concentration. Punicalagin (Sigma-Aldrich, P0023) and Rutin (Sigma-Aldrich, PHL89270) were dissolved in DMSO to reach a concentration of 10 mM, and the solution was diluted to the appropriate amount in CM before use. The final concentration of DMSO in all treatment wells was 0.1% (*v*/v). Cells were pre-treated with punicalagin and rutin 24 h before UVA irradiation. Cells that were not treated with compounds or not exposed to UVA radiation served as controls.

2.3. Fluorescence lifetime imaging microscopy (FLIM)

FLIM data were acquired with a Nikon A1-MP confocal microscope equipped with a 2-photon Ti:Sapphire laser (Mai Tai, Spectra Physics, Newport Beach, CA) by producing 80-fs pulses at a repetition rate of 80 MHz. A PML-SPEC 16 GaAsP (B&H, Germany) multi-wavelength detector coupled to a SPC-830 TCSPC/FLIM device (B&H, Germany) was used to collect the decay data. A 60 × oil-immersion objective, 1.2 NA, was used for all experiments. Samples were excited at 750 nm. FLIM signals were acquired in the spectral range from 408 to 508 nm, with an image resolution of 512 × 512.

2.4. Fis1 and Mitofusin2 levels detection

Quantification of human Fission 1 protein (Fis1) and Mitofusin-2 (MFN2) was performed in fibroblast protein lysates using two independent sandwich ELISA kits, one specific for Fis1 (MBS453299) and one for MFN2 (MBS2024886) (MyBioSource Inc., San Diego, CA, USA), following the manufacturer's protocols. Cells were collected 24 h after the 2-h UVA irradiation period. After lysis, cell debris was removed by centrifugation, and protein concentration in the supernatants was determined using a colorimetric protein assay in 96-well microplates (Bio-Rad, Hercules, CA, USA) to ensure equal protein loading across all samples.For each ELISA kit, standards were prepared by serial dilution to generate a seven-point calibration curve. Aliquots of 50 μL of standards or samples (cell lysates at a protein concentration of 0.5 mg/mL) were loaded in triplicate into wells pre-coated with the corresponding capture antibody. After sample incubation and washing, the biotin-conjugated detection antibody and HRP-streptavidin reagents supplied with each kit were added sequentially. Chromogenic development was carried out using TMB substrate, and the reaction was stopped with sulfuric acid. Absorbance was measured at 450 nm using a microplate reader. Fis1 and MFN2 concentrations were calculated in ng/mL by interpolating absorbance values on the respective standard curves and expressed as percentage of the untreated, non-irradiated control (CTRL = 100%). Each experiment was repeated at least three times, with up to eight technical replicates per condition. Data are presented as mean ± SEM. Statistical analyses were performed using one-way ANOVA in GraphPad Prism v.8 (San Diego, CA, USA), with significance set at $p \leq 0.05$.

2.5. Phasor image analysis

The analysis of the FLIM curves and the evaluation of metabolic and oxidative stress within cells was performed using the phasor algorithm [31].Each pixel of a FLIM image contains an array of values representing the decay curve (Fig. 2 A-B). Phasor analysis enables to associate the information contained in the array into a couple of values representing the real and imaginary parts of the normalized Fourier Transform, i.e. g and s [32]. These coordinates are computed for each pixel using the following equations:

$$g = \frac{n\sum_{k=1}^{n} I_k\left(\cos\left(\frac{2\pi k}{n}\right) - \cos\left(\frac{2\pi(k-1)}{n}\right)\right)}{2\pi\sum_{k=1}^{n} I_k} \quad (1)$$

$$s = \frac{n\sum_{k=1}^{n} I_k\left(\sin\left(\frac{2\pi k}{n}\right) - \sin\left(\frac{2\pi(k-1)}{n}\right)\right)}{2\pi\sum_{k=1}^{n} I_k} \quad (2)$$

Where I_k indicates the k-th element of the intensity emission profile. These pair of values can be represented as a unique point in a plane referred to as the phasor diagram (Fig. 2C), providing a model-free analytical framework for the analysis of FLIM data that obviates the need for explicit mathematical fitting models. Notably, a single exponential decay is mapped onto a point on the universal semicircle of the phasor diagram [33] (Fig. 2E). In contrast, multi-exponential decay profiles yield phasor points that are linear combinations of individual

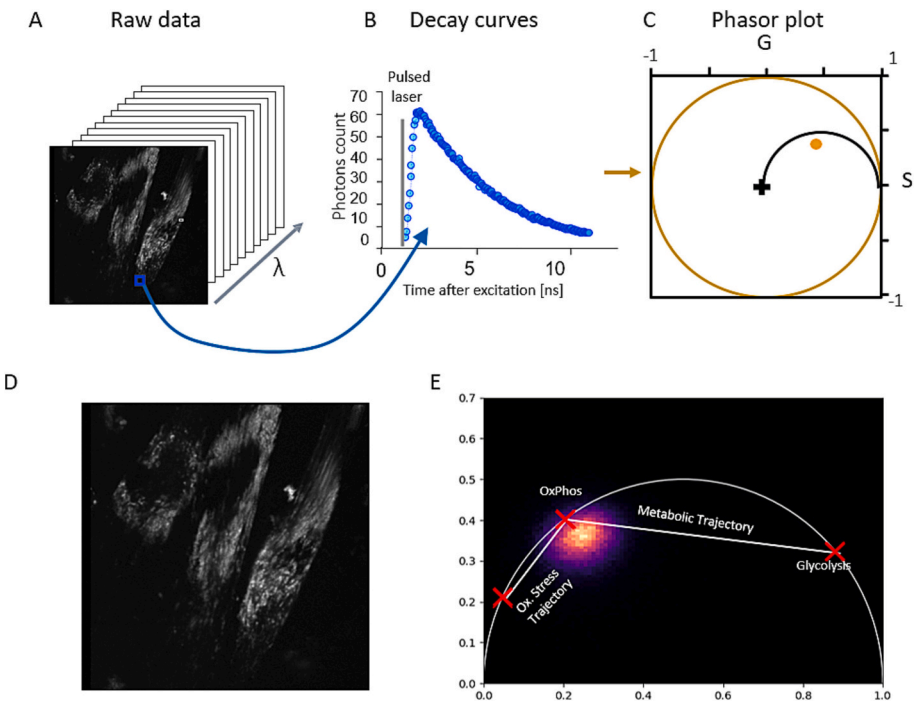

Fig. 2. Phasor-Based FLIM. (A–C) *Theoretical framework.* (A) Each voxel of the FLIM dataset contains a complete fluorescence decay profile, acquired by integrating time-resolved emission signals over multiple wavelengths. The stack of images represents the temporal evolution of fluorescence decay for each pixel. (B) Example of a representative decay curve from the pixel highlighted in (A), showing photon counts as a function of time after pulsed laser excitation and illustrating the characteristic multiexponential nature of cellular autofluorescence. (C) Transformation of the decay data into the phasor domain, where each pixel's fluorescence lifetime is mapped onto a single point (yellow) in the phasor plot defined by the real (G) and imaginary (S) coordinates of the normalized Fourier transform. Points located on the semicircle correspond to single-exponential decays, whereas multiexponential decays fall within the semicircle as linear combinations of lifetime components. (D–E) *Experimental application.* (D) Representative FLIM image from the analyzed dataset, showing subcellular lifetime heterogeneity across fibroblast structures. (E) Phasor plot representing the distribution of all image pixels as a dense cloud along the metabolic trajectory (white line) between glycolysis (right red cross) and oxidative phosphorylation (left red cross). The lower left region identifies an additional trajectory associated with long-lifetime species related to oxidative stress. The colour scale encodes pixel density within the phasor space. (For interpretation of the references to colour in this figure legend, the reader is referred to the web version of this article.)

exponential components, the so-called law of addition. Therefore, the ensemble of such phasors forms a convex region confined within the semicircle, encompassing all possible linear combinations of distinct lifetime components [34].Consequently, a heterogeneous fluorescence lifetime distribution within an image result in a cloud of phasor points dispersed across the diagram.

In biological systems with multiple contributions to autofluorescence signals fluorophores, such as tissues, the global decay profile is represented by a phasor that constitutes the weighted sum of the individual phasors of each fluorophore:

$$g = \sum_n f_n g_n \tag{3}$$

$$s = \sum_n f_n s_n \tag{4}$$

$$\sum_n f_n = 1 \tag{5}$$

Where f_n is the fractional contribution of n-th species. When two molecular species exhibit distinct multi-exponential decay characteristics, their respective phasors define two discrete locations within the diagram. The weighted combinations of these species lie along a linear trajectory connecting the two phasor points. For three-component systems, the phasor distribution is enclosed within a triangular region, with vertices corresponding to the phasors of the pure components. More generally, an N-component system generates a phasor distribution constrained within an N-sided polygon, whose vertices correspond to the individual species' phasors. A custom Python script was employed to perform phasor-based lifetime analysis, facilitating the investigation of metabolic pathways. Given the fundamental role of free NADH (~0.4 ns) and protein-bound NADH (~3.4 ns) lifetimes fall along a linear trajectory (the "metabolic trajectory") on the phasor plot and reflect cellular metabolic states, particularly oxidative phosphorylation (OXPHOS) activity. FLIM detects the combined autofluorescence of NADH and NADPH. A third distinct population, characterized by a long lifetime of approximately 7.8 ns, was identified as a marker of lipid peroxidation and plotted along a separate line (the "oxidative stress axis"). To simultaneously assess both metabolic activity and oxidative stress, cells (e.g., HeLa) or freshly excised tissues (e.g., white adipose tissue) were imaged under label-free conditions [31]. To quantify metabolic and oxidative shifts, we introduced two phasor-derived parameters: F_{ox}, representing the fractional contribution of long-lifetime components related to oxidative stress, and F_{oxphos} predominantly indicating the proportion of protein-bound NADH species, which reflect mitochondrial oxidative phosphorylation activity [35,36](Fig. 2E). In our analysis, only the nuclear region was excluded from the phasor-FLIM evaluation to prevent fluorescence lifetime artefacts arising from chromatin and nucleic acid signals. The mitochondria and cytoplasmic compartments were fully included within the region of interest. Consequently, F_{oxphos}reflects the contribution of protein-bound NAD(*P*)H associated with mitochondrial oxidative metabolism, while F_{ox}represents the fraction of long-lifetime components related to oxidative stress. This approach follows the methodological framework described by Datta et al. [31], which enables label-free mapping of intracellular metabolic states without the need for exogenous markers. These values were extracted from the phasor cloud based on reference trajectories

corresponding to known fluorescence lifetime components. The phasor clusters corresponding to NADH and the long-lifetime species were identified using cursors on the phasor plot and mapped back onto the spatial fluorescence image to reveal their subcellular localization. This multimodal, non-invasive method allows the concurrent monitoring of OXPHOS status and oxidative lipid damage in live or fixed biological samples.

For statistical evaluation, a Kruskal-Wallis test was initially performed to assess group differences, revealing significant effects for both parameters: F_{oxphos}(H = 15.510, $p = 0.0084$) and F_{ox} (H = 14.714, $p = 0.0117$). Post hoc comparisons were then conducted using Dunn's test to identify significant pairwise differences between experimental groups.

3. Results

3.1. Mitochondrial fusion and fission

Mitochondrial fusion and fission activity was assessed using an ELISA assay by measuring the levels of Mitofusin 2 (MFN2), a mitochondrial membrane protein involved in fusion, and Fis1, a component of the mitochondrial complex known as the ARCosome, which promotes mitochondrial fission. Protein levels were evaluated 2 h after UVA irradiation (UVA dose of 0.432 J/cm^2) of fibroblasts that had been pre-treated with both punicalagin and rutin, as shown in Fig. 3. As expected, Fis1 levels significantly increased following UVA exposure, indicating mitochondrial damage. However, Fis1 levels returned to baseline in cells pre-treated with punicalagin and rutin, demonstrating the protective effects of both compounds against UVA-induced stress. Conversely, MFN2 levels decreased after UVA irradiation, consistent with reduced mitochondrial fusion activity. Pre-treatment with punicalagin and rutin prior to irradiation led to an increase in MFN2 expression, approaching control levels.

3.2. Analysis of UVA induced lipid peroxidation

As shown in Fig. 4, all pairwise comparisons among the experimental groups (Kruskal–Wallis with Dunn's post-hoc test) revealed distinct oxidative profiles across treatments. Pretreatment with punicalagin (PUN) significantly reduced oxidative stress under basal conditions, decreasing $F_{o\times}$ from 0.179 ± 0.05 (CTRL) to 0.057 ± 0.02 ($p = 0.029$). Rutin (RUT) also reduced $F_{o\times}$ relative to CTRL (0.140 ± 0.01), although this effect was not statistically significant ($p = 0.530$). The direct comparison between the two polyphenols under basal conditions showed a non-significant trend toward a stronger antioxidant activity of PUN (PUN vs RUT: 0.057 ± 0.02 vs 0.140 ± 0.01; $p = 0.094$). As expected, UVA irradiation increased $F_{o\times}$ when compared to PUN alone (UVA vs PUN: 0.243 ± 0.01 vs 0.057 ± 0.02; $p = 0.001$), validating the irradiated condition as a positive control. Importantly, PUN markedly reduces $F_{o\times}$ under basal conditions, and the significant increase observed when UVA is added (PUN vs PUN + UVA: 0.057 ± 0.02 → 0.236 ± 0.02; $p = 0.003$) shows that UVA largely abolishes the basal protection. AA similar pattern was observed for RUT. Under UVA exposure, RUT pretreatment reduced $F_{o\times}$ relative to UVA alone (RUT+UVA vs UVA: 0.129 ± 0.02 vs 0.243 ± 0.01), showing a protective trend close to statistical significance ($p = 0.062$). Finally, the comparison between the two polyphenols under irradiation revealed that RUT tended to provide stronger protection than PUN (RUT+UVA vs PUN+UVA: 0.129 ± 0.02 vs 0.236 ± 0.02; $p = 0.110$), although the difference did not reach statistical significance. Overall, these data confirm that both compounds exert antioxidant activity, with PUN being more effective under basal conditions and RUT showing a comparatively stronger trend under UVA-induced oxidative stress.

3.3. Analysis of metabolic trajectories

As shown in Fig. 5, phasor-based FLIM analysis of the extranuclear compartment showed that oxidative phosphorylation (F_{oxphos}) is the

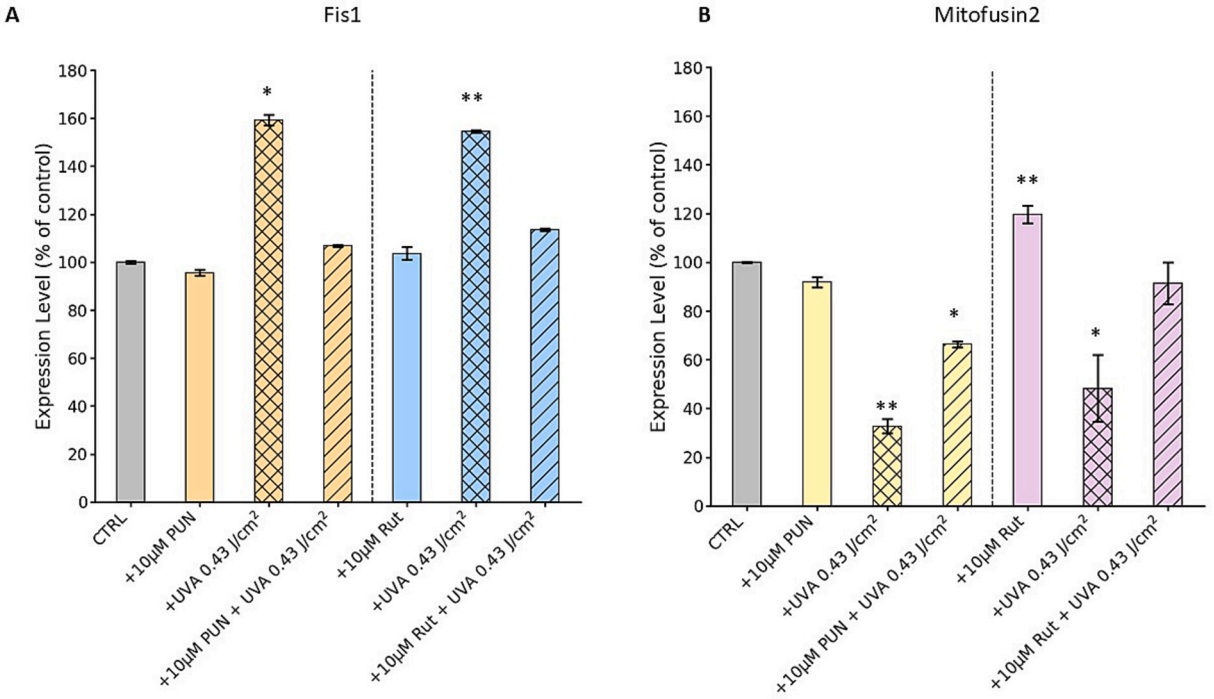

Fig. 3. Fis1 and MFN2 levels after 2 h of UVA irradiation with and without 10 μM of punicalagin and rutin. ELISA-based quantification of Fis1 and MFN2 protein levels is shown. Data are expressed as mean ± SEM and presented as percentage of the untreated control (CTRL, set as 100%). Experiment was repeated three times with up to eight technical replicates per condition. The two "+UVA 0.43 J/cm^2 " groups represent the UVA-irradiated controls for the punicalagin and rutin experimental series, which were performed independently. UVA exposure increased Fis1 and reduced MFN2 levels, pre-treatment with punicalagin or rutin was associated with a partial normalization of Fis1 and MFN2 levels toward control values. * $p < 0.05$, ** $p < 0.01$ vs. CTRL.

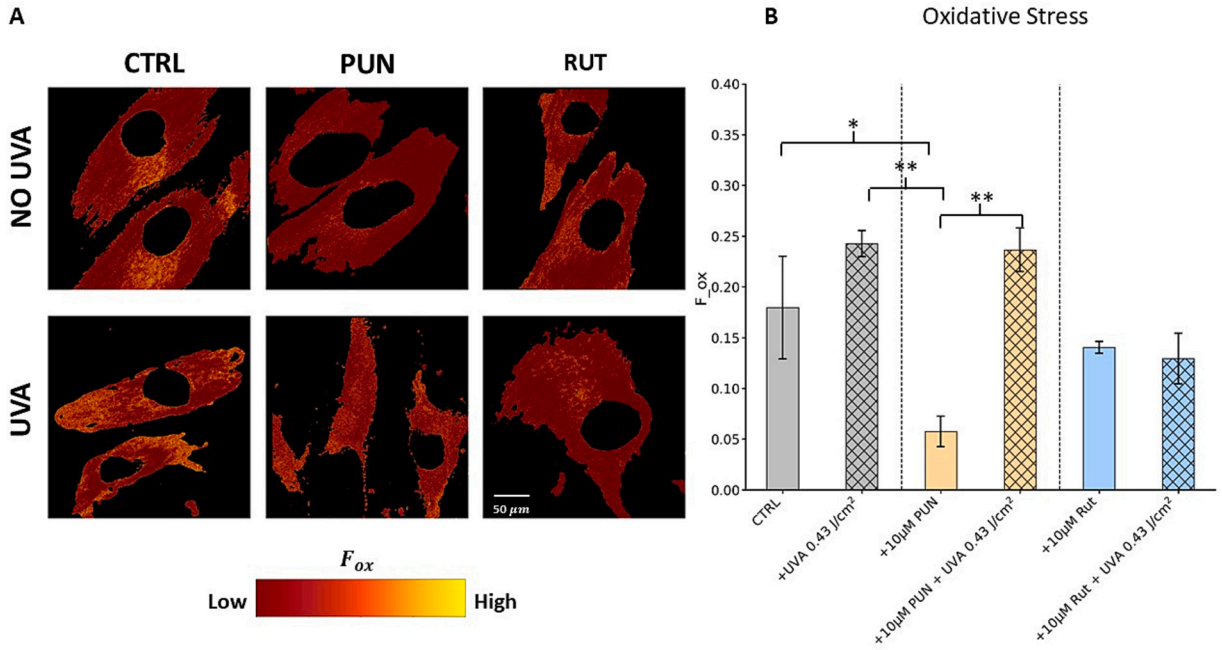

Fig. 4. Phasor-based analysis of oxidative stress in human dermal fibroblasts under different treatments. (A) Representative phasor-fraction images of whole cells (nucleus excluded) showing oxidative stress distribution. The colour gradient from red (low) to yellow (high) represents the oxidative stress fraction (F_o×). Scale bar: 50 μm. (B) Quantification of F_o× values under each condition (mean ± SEM, from three experiments). Orange bars: punicalagin (10 μM); blue bars: rutin (10 μM). Solid bars: no UVA; patterned bars: UVA dose of 0.432 J/cm^2; *p < 0.05; **p < 0.01. (For interpretation of the references to colour in this figure legend, the reader is referred to the web version of this article.)

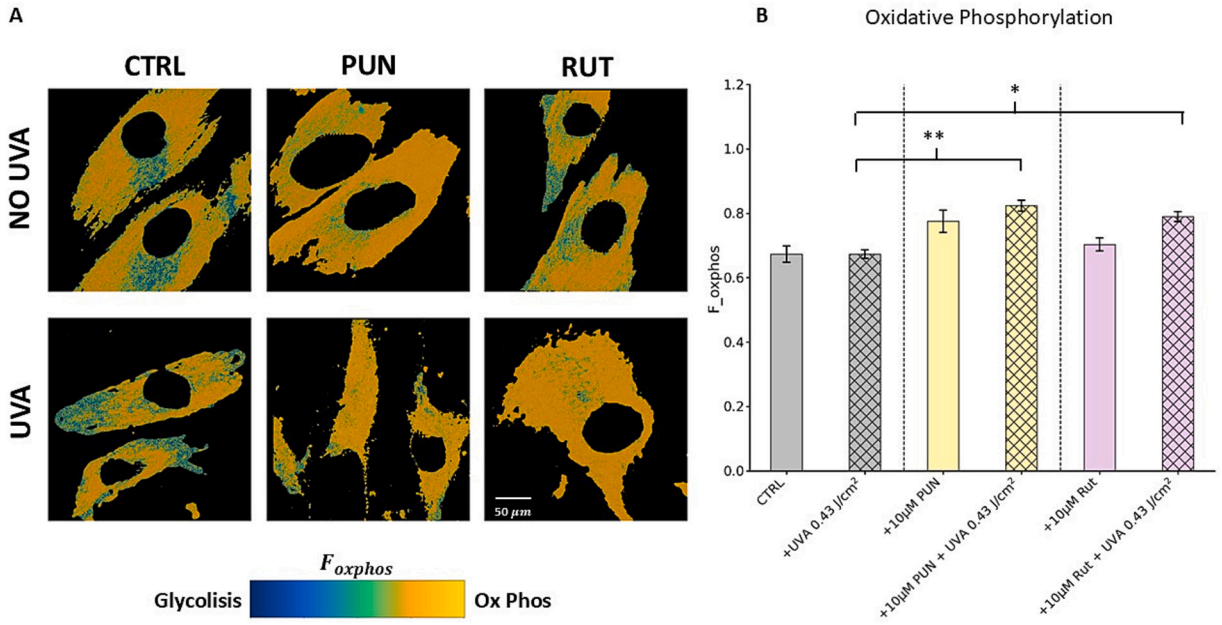

Fig. 5. Phasor-based analysis of metabolic balance between glycolysis and oxidative phosphorylation (OxPhos) in human dermal fibroblasts under different treatments. (A) Representative phasor-fraction images of of whole cells (excluding nuclei)) showing the glycolytic–OxPhos balance. The colour gradient from blue (glycolysis-dominant) to yellow (OxPhos-dominant) indicates the metabolic fraction (F_{OxPhos}). Scale bar: 50 μm. (B) Quantification of F_{OxPhos} values under each condition (mean ± SEM; from three experiments). Yellow bars: punicalagin (10 μM); purple bars: rutin (10 μM). Solid bars: no UVA; patterned bars: UVA dose of 0.432 J/cm^2; p < 0.05; **p < 0.01. (For interpretation of the references to colour in this figure legend, the reader is referred to the web version of this article.)

predominant metabolic pathway in basal conditions (CTRL: 0.673 ± 0.02). Under non-irradiated conditions, punicalagin (PUN) tended to increase F_{oxphos} (0.775 ± 0.03; p = 0.057), whereas rutin (RUT) produced no significant change (0.703 ± 0.02; p = 0.567). These contrasts quantify the intrinsic metabolic action of each polyphenol in the absence of oxidative stress. UVA irradiation alone did not reduce oxidative phosphorylation (CTRL: 0.673 ± 0.02 → UVA: 0.673 ± 0.01; p = 0.945), indicating that the UVA dose used increases oxidative stress without suppressing mitochondrial respiration. When polyphenols were added before UVA exposure, both compounds preserved mitochondrial activity relative to UVA alone. PUN + UVA significantly increased F_{oxphos} compared with UVA (0.823 ± 0.02 vs 0.673 ± 0.01; p = 0.004), and

RUT + UVA produced a similar enhancement (0.789 ± 0.02 vs 0.673 ± 0.01; $p = 0.023$), confirming their protective effect on oxidative metabolism. Within-compound comparisons revealed different biological patterns. RUT became metabolically more effective under stress (RUT: 0.703 ± 0.02 → RUT + UVA: 0.789 ± 0.02; $p = 0.073$), while PUN maintained its basal metabolic effect during irradiation (PUN: 0.775 ± 0.03 → PUN + UVA: 0.823 ± 0.02; $p = 0.260$). Overall, both compounds preserved oxidative phosphorylation under UVA-induced oxidative stress, but with distinct behaviors: PUN exhibited its strongest metabolic effect under basal conditions, whereas RUT enhanced mitochondrial activity predominantly under stress.

4. Discussion

Our findings offer a comprehensive view of how rutin and punicalagin protect human dermal fibroblasts from UVA-induced damage by targeting three interconnected domains: oxidative balance, mitochondrial metabolism, and organelle homeostasis. These aspects are functionally linked, and modulation of one often affects the others. In this study, organelle morphology was not directly examined; instead, functional states were inferred from molecular and metabolic indicators. Mitochondrial activity was assessed through the expression of fission (Fis1) and fusion (MFN2) proteins, which regulate mitochondrial dynamics, together with the phasor-FLIM–derived parameters that reflects oxidative phosphorylation activity based on NAD(*P*)H lifetime signatures. Phasor-FLIM analysis of oxidative stress confirmed the well-established pro-oxidant effect of UVA (in Fig. 4), with the F_{ox} parameter increasing from 0.179 ± 0.05 in CTRL to 0.243 ± 0.01 under UVA exposure, corresponding to a 36% increase. Although this increase did not reach statistical significance ($p = 0.301$), it represents a trend toward higher oxidative stress after UVA exposure. Pretreatment with PUN markedly reduced basal oxidative stress to 0.057 ± 0.02 (68% reduction vs CTRL, $p = 0.029$), while RUT decreased F_{ox} to 0.140 ± 0.01 (22% reduction, not significant). Under UVA challenge, RUT pretreatment provided substantial protection, lowering F_{ox} to 0.129 ± 0.02, while PUN pretreatment showed modest effects (0.236 ± 0.02).

Although not statistically significant, the near-significant reduction observed for RUT ($p = 0.062$) consistently indicated a protective trend that was reproduced across experiments and is now explicitly reported in the Results. The direct comparison between PUN and RUT under irradiation (PUN + UVA vs RUT + UVA) did not reach statistical significance ($p = 0.110$), suggesting that although RUT shows a stronger trend under UVA stress, future studies will be required to determine whether this represents a true biological difference.

In parallel, metabolic profiling of oxidative phosphorylation (OxPhos in Fig. 5) revealed that control cells exhibited an F_{oxphos} of 0.673 ± 0.02, reflecting a predominant reliance on oxidative metabolism.

The UVA dose used in this study did not reduce mitochondrial OxPhos (CTRL vs UVA, $p = 0.945$), an effect expected for this controlled dose (0.432 J/cm^2), which induces oxidative stress without impairing mitochondrial respiration. This feature of the model is essential, as it allows assessing whether polyphenols actively preserve OxPhos under oxidative challenge rather than recovering from mitochondrial dysfunction. Pretreatment with polyphenols enhanced oxidative metabolism: PUN increased F_{oxphos} to 0.775 ± 0.03 ($p = 0.057$ vs CTRL), while RUT yielded a modest increase to 0.703 ± 0.02 ($p = 0.567$). Importantly, the combination of polyphenols with UVA further boosted oxidative metabolism. Cells treated with PUN + UVA reached an F_{oxphos} of 0.823 ± 0.02 (+22% $p = 0.004$ vs UVA), while RUT + UVA reached 0.789 ± 0.02 (+17% $p = 0.023$ vs UVA).

At the functional level, UVA triggered substantial mitochondrial fragmentation, as evidenced by a 75% rise in fission protein Fis1 and a 55% decrease in the fusion protein MFN2(Fig. 3A–B). Rutin effectively counteracted these alterations by normalizing the expression levels of Fis1 and MFN2, suggesting a restoration of balanced mitochondrial balance. In contrast, punicalagin did not significantly modify MFN2 expression, consistent with its limited influence on mitochondrial fusion processes. This observation is in line with the data shown in Fig. 3B, which display only a partial recovery of MFN2 levels in punicalagin-pretreated cells, whereas Fis1 reduction indicates a protective modulation mainly acting on fission-related pathways. Punicalagin exerted only partial protection, leading to a moderate recovery of fusion activity and a slight attenuation of fission. Under UVA stress, rutin pretreatment maintained mitochondrial structure more efficiently, whereas punicalagin provided only incomplete rescue. These results suggest that rutin and punicalagin act through distinct but complementary mechanisms. Rutin exerts a broader upstream protective effect, attenuating oxidative stress, restoring mitochondrial fusion, and supporting redox homeostasis. Punicalagin, in contrast, acts more downstream, primarily enhancing oxidative phosphorylation efficiency, even in structurally compromised mitochondria, a pattern consistent with metabolic compensation rather than morphological preservation. This compartment-specific distinction is consistent with previously described molecular pathways [16,17] Rutin is known to activate Nrf2-mediated antioxidant responses, promoting the expression of detoxifying enzymes. Punicalagin, on the other hand, has been shown to scavenge ROS and support mitochondrial respiration by preserving membrane potential and electron transport chain [16,26]. In human dermal fibroblasts, our previous data show that both compounds protect mitochondrial function and oxidative balance under UVA stress. Mitochondrial dynamics are time-dependent: protein changes occur early but are most pronounced 24 h after UVA exposure, when cellular responses are consolidated. This suggests rutin and punicalagin's protective effects go beyond immediate antioxidant action to restoring mitochondrial balance over time [16,17].

Our present data further support previous findings, indicating that rutin may modulate the expression of mitochondrial dynamics regulators, thereby indirectly influencing mitochondrial function. Phasor-FLIM imaging further revealed that lipid peroxidation is not confined to mitochondria but is also prominent in other cytoplasmic compartments. This pattern suggests that organelles such as the endoplasmic reticulum and peroxisomes, both involved in lipid metabolism and detoxification, may also be targets of UVA-induced oxidative stress. The ability of both polyphenols to attenuate F_{ox} in these regions underscores their potential to offer broader cytoplasmic protection. Overall, our findings emphasize that mitochondrial dynamics and metabolism are functionally intertwined but can be differentially modulated by distinct polyphenols. Rutin primarily preserves redox balance and supports mitochondrial functional integrity, whereas punicalagin enhances oxidative metabolism, possibly compensating for partial structural alterations. These complementary mechanisms align with previous studies showing polyphenol-mediated regulation of mitochondrial performance and redox signaling. Together, they highlight polyphenols as precision nutraceuticals capable of stabilizing cellular homeostasis under photo-oxidative stress. Rutin primarily preserves redox balance and mitochondrial integrity, while punicalagin enhances bioenergetic performance. Together, they represent two synergistic strategies for protecting skin cells from UVA-induced damage. Our results align with literature showing polyphenols enhance cellular resilience across tissues and stress types (for a review see [37]). In future studies combination of both polyphenols in pretreatment of UVA exposed fibroblasts could be considered.

Despite the encouraging outcomes, it is important to clearly recognize the limitations of this study. All experiments were performed using fibroblasts derived from a single healthy donor, which restricts the extent to which the results can be extrapolated to a broader population. Furthermore, although FLIM-phasor analysis represents a powerful and non-invasive approach to monitor redox and metabolic states, it does not allow the direct identification of specific ROS species or the reconstruction of intracellular signaling pathways. To overcome these constraints, future work should integrate metabolomics, transcriptomics

and proteomic analyses to better elucidate the mechanisms underlying skin and systemic photoprotection. In addition, since UVA-induced skin damage also involves inflammation and extracellular matrix remodelling, validation in in vivo models will be necessary to fully assess the translational potential of these polyphenols in preventing photoaging and photocarcinogenesis.

5. Conclusions

This study demonstrates that rutin and punicalagin offer significant protection against UVA-induced oxidative and metabolic stress in human dermal fibroblasts, acting through distinct but complementary mechanisms. Rutin showed broad-spectrum efficacy by markedly reducing oxidative stress, restoring mitochondrial morphology, and enhancing oxidative metabolism. Notably, lipid peroxidation was also observed in non-mitochondrial compartments, suggesting that rutin provides wider cytoplasmic protection beyond the mitochondria. Punicalagin was less effective in preserving mitochondrial structure but strongly enhanced oxidative phosphorylation, indicating a role in metabolic adaptation under stress, likely to support ATP production despite partial organelle damage. Overall, rutin emerges as the more comprehensive photoprotective agent, offering both structural and metabolic resilience. Punicalagin, while more limited in scope, may still be valuable for sustaining energy metabolism in oxidative conditions. By integrating phasor-FLIM imaging with molecular markers of mitochondrial dynamics, this study provides a detailed subcellular perspective on the protective actions of polyphenols. These findings highlight how polyphenols can act as targeted modulators of oxidative and metabolic vulnerabilities in the skin. The distinct subcellular effects of rutin and punicalagin highlight their capacity to selectively modulate cellular responses to photo-oxidative stress. Based on our in-vitro findings, both compounds emerge as promising candidates for topical strategies aimed at strengthening skin resilience to UVA-induced damage, with rutin exhibiting the most comprehensive protective profile. While systemic implications cannot be inferred from the present data, the molecular mechanisms identified here may nonetheless provide a basis for future studies exploring whether these polyphenols also hold relevance in broader nutraceutical contexts.

Authors contribution

Conceptualization, G.M., A.R. and F.D.G.; Methodology, A.R., F.D.G., G.M., M.M.D.G., B.N., E.T., M.E.C. and M.D.S.; Software, A.R., F.D.G. and G.M.; Validation, A.R., F.D.G., G.M., M.M.D.G., B.N., E.T., M.E.C. and M.D.S.; Formal analysis, G.M., A.R, and F.D.G.; Investigation, A.R., F.D.G., G.M., M.M.D.G., B.N., E.T., M.E.C. and M.D.S.; Resources, A.R., F.D.G. and G.M.; Data curation, A.R., F.D.G. and G.M.; Writing—original draft preparation, A.R., F.D.G. and G.M.; Writing— review and editing, A.R., F.D.G. and G.M.; Visualization, A.R., F.D.G. and G.M.; Supervision, G.M.; Project administration, G.M.; Funding acquisition, G.M. All authors have read and agreed to the published version of the manuscript.

CRediT authorship contribution statement

Alessia Riente: Writing – review & editing, Writing – original draft, Visualization, Validation, Software, Resources, Methodology, Investigation, Formal analysis, Data curation, Conceptualization. **Flavio Di Giacinto:** Writing – review & editing, Writing – original draft, Visualization, Validation, Software, Resources, Methodology, Investigation, Data curation, Conceptualization. **Michele Maria De Giulio:** Validation, Methodology, Investigation. **Benedetta Niccolini:** Validation, Methodology, Investigation. **Elisabetta Tabolacci:** Validation, Methodology, Investigation. **Maria Elisabetta Clementi:** Validation, Methodology, Investigation. **Marco De Spirito:** Validation, Methodology, Investigation. **Giuseppe Maulucci:** Writing – review & editing, Writing – original draft, Visualization, Validation, Supervision, Software, Resources, Project administration, Methodology, Investigation, Funding acquisition, Formal analysis, Data curation, Conceptualization.

Ethics approval statement

The study was conducted in accordance with the Declaration of Helsinki and approved by the Ethics Committee of Università Cattolica del Sacro Cuore- ID 3147.

Funding

This project was supported in part by a research grant awarded to GM from Regione Lazio PO FSE 2014–2020 ('QUaD2: Una piattaforma e-Health potenziata da algoritmi di machine learning QUantistico per la prevenzione di complicazioni macrovascolari e microvascolari nel Diabete di tipo 2'), co-funded by Blu Sistemi s.r.l., and by a research grant awarded to GM by Università Cattolica del Sacro Cuore – Linea D1 2021. Università Cattolica del Sacro Cuore also contributed to the funding of this research project and its publication (D3.1 2025).

Declaration of competing interest

The authors declare that they have no known competing financial interests or personal relationships that could have appeared to influence the work reported in this paper.

Data availability

Data will be made available on request.

References

[1] R.M. Lucas, et al., Human health in relation to exposure to solar ultraviolet radiation under changing stratospheric ozone and climate, Photochem. Photobiol. Sci. 18 (3) (2019) 641–680, https://doi.org/10.1039/C8PP90060D.
[2] J. Krutmann, Ultraviolet A Radiation-induced Biological Effects in Human Skin: Relevance for Photoaging and Photodermatosis [Online]. Available, www.elsevier.com/locate/jdermsci, 2000.
[3] F. Bernerd, T. Passeron, I. Castiel, C. Marionnet, The damaging effects of long UVA (UVA1) rays: a major challenge to preserve skin health and integrity, Int. J. Mol. Sci. (2022 Aug 01), https://doi.org/10.3390/ijms23158243.
[4] L.H.F. Mullenders, Solar UV Damage to Cellular DNA: From Mechanisms to Biological Effects, Royal Society of Chemistry, 2018, https://doi.org/10.1039/c8pp00182k.
[5] J. Cadet, T. Douki, Formation of UV-Induced DNA Damage Contributing to Skin cancer Development, Royal Society of Chemistry, 2018, https://doi.org/10.1039/c7pp00395a.
[6] R. Bosch, et al., Mechanisms of photoaging and cutaneous photocarcinogenesis, and photoprotective strategies with phytochemicals, Antioxidants (2015 Jun 01), https://doi.org/10.3390/antiox4020248.
[7] S.G. Jin, F. Padron, G.P. Pfeifer, UVA Radiation, DNA Damage, and Melanoma, Am. Chem. Soc. (2022 Sep 20), https://doi.org/10.1021/acsomega.2c04424.
[8] A. Negre-Salvayre, R. Salvayre, Post-translational modifications evoked by reactive carbonyl species in ultraviolet-A-exposed skin: implication in fibroblast senescence and skin photoaging, Antioxidants (2022 Nov 01), https://doi.org/10.3390/antiox11112281.
[9] A.K. von Thaler, Y. Kamenisch, M. Berneburg, The role of ultraviolet radiation in melanomagenesis, Exp. Dermatol. (2010 Feb), https://doi.org/10.1111/j.1600-0625.2009.01025.x.
[10] I.V. Ivanov, T. Mappes, P. Schaupp, C. Lappe, S. Wahl, Ultraviolet radiation oxidative stress affects eye health, J. Biophotonics (2018 Jul 01), https://doi.org/10.1002/jbio.201700377.
[11] B.A. Gilchrest, Photoaging, J. Invest. Dermatol. 133 (2013 Jul) E2–E6, https://doi.org/10.1038/skinbio.2013.176.
[12] A. Kammeyer, R.M. Luiten, Oxidation events and skin aging, Ageing Res. Rev. (2015 May 01), https://doi.org/10.1016/j.arr.2015.01.001.
[13] D. Xian, R. Lai, J. Song, X. Xiong, J. Zhong, Emerging perspective: role of increased ROS and redox imbalance in skin carcinogenesis, Oxidative Med. Cell. Longev. (2019), https://doi.org/10.1155/2019/8127362.
[14] C. Garg, H. Sharma, M. Garg, Skin photo-protection with phytochemicals against photo-oxidative stress, photo-carcinogenesis, signal transduction pathways and extracellular matrix remodeling—an overview, Ageing Res. Rev. (2020 Sep 01), https://doi.org/10.1016/j.arr.2020.101127.
[15] M. Abbas, et al., Natural polyphenols: an overview, Int. J. Food Prop. (2017 Aug 03), https://doi.org/10.1080/10942912.2016.1220393.

[16] E. Tabolacci, et al., Rutin protects fibroblasts from UVA radiation through stimulation of Nrf2 pathway, Antioxidants 12 (4) (2023 Apr), https://doi.org/10.3390/antiox12040820.
[17] G. Bianchetti, P. Bottoni, G. Tringali, G. Maulucci, E. Tabolacci, M.E. Clementi, The polyphenolic compound punicalagin protects skin fibroblasts from UVA radiation oxidative damage, Curr. Res. Pharmacol. Drug Discov. 6 (2024 Jan), https://doi.org/10.1016/j.crphar.2024.100186.
[18] Abhratanu Ganguly, et al., Unveiling the protective efficacy of rutin against high-sucrose diet-induced oxidative stress, biochemical alterations, and organismal hazards in *Drosophila melanogaster*, Toxicol. Res. (Camb.) 14 (4) (2025 Aug).
[19] Y. Liu, et al., Dietary polyphenols as anti-aging agents: targeting the hallmarks of aging, Nutrients (2024 Oct 01), https://doi.org/10.3390/nu16193305. Multidisciplinary Digital Publishing Institute (MDPI).
[20] A. Rak-Pasikowska, K. Hałucha, M. Kamińska, J. Niewiadomska, A. Noszczyk-Nowak, I. Bil-Lula, The effect of pomegranate peel extract on the oxidative and inflammatory status in the spleens of rats with metabolic syndrome, Int. J. Mol. Sci. 25 (22) (2024 Nov), https://doi.org/10.3390/ijms252212253.
[21] S.K. Panchal, H. Poudyal, T.V. Arumugam, L. Brown, Rutin attenuates metabolic changes, nonalcoholic steatohepatitis, and cardiovascular remodeling in high-carbohydrate, high-fat diet-fed rats, J. Nutr. 141 (6) (2011 Jun) 1062–1069, https://doi.org/10.3945/jn.111.137877.
[22] W.C. Huang, et al., Punicalagin from pomegranate ameliorates TNF-α/IFN-γ-induced inflammatory responses in HaCaT cells via regulation of SIRT1/STAT3 axis and Nrf2/HO-1 signaling pathway, Int. Immunopharmacol. 130 (2024 Mar), https://doi.org/10.1016/j.intimp.2024.111665.
[23] A. Gęgotek, P. Domingues, E. Skrzydlewska, Natural exogenous antioxidant defense against changes in human skin fibroblast proteome disturbed by UVA radiation, Oxidative Med. Cell. Longev. 2020 (2020), https://doi.org/10.1155/2020/3216415.
[24] S. Rahmani, K. Naraki, A. Roohbakhsh, A.W. Hayes, G. Karimi, The protective effects of rutin on the liver, kidneys, and heart by counteracting organ toxicity caused by synthetic and natural compounds, Food Sci. Nutr. (2023 Jan 01), https://doi.org/10.1002/fsn3.3041.
[25] D.E. Rotimi, T.C. Elebiyo, O.A. Ojo, Therapeutic potential of rutin in male infertility: a mini review, J. Integr. Med. (2023 Mar 01), https://doi.org/10.1016/j.joim.2023.01.004.
[26] Y. Qing Sun, X. Tao, X. Ming Men, Z. Wei Xu, T. Wang, In vitro and in vivo antioxidant activities of three major polyphenolic compounds in pomegranate peel: Ellagic acid, punicalin, and punicalagin, J. Integr. Agric. 16 (8) (2017 Aug) 1808–1818, https://doi.org/10.1016/S2095-3119(16)61560-5.
[27] M.P. Murphy, How mitochondria produce reactive oxygen species, Biochem. J. (2009 Jan 01), https://doi.org/10.1042/BJ20081386.
[28] M. Kciuk, B. Marciniak, M. Mojzych, R. Kontek, Focus on uv-induced dna damage and repair—disease relevance and protective strategies, MDPI AG (2020 Oct 01), https://doi.org/10.3390/ijms21197264.
[29] L.A. Sena, N.S. Chandel, Physiological roles of mitochondrial reactive oxygen species, Mol. Cell (2012 Oct 26), https://doi.org/10.1016/j.molcel.2012.09.025. Cell Press.
[30] A. Besaratinia, et al., DNA Lesions Induced by UV A1 and B Radiation in Human Cells: Comparative Analyses in the Overall Genome and in the p53 Tumor Suppressor Gene [Online]. Available, https://www.pnas.org, 2005.
[31] R. Datta, A. Alfonso-Garciá, R. Cinco, E. Gratton, Fluorescence lifetime imaging of endogenous biomarker of oxidative stress, Sci. Rep. 5 (2015 May), https://doi.org/10.1038/srep09848.
[32] S.-C. Liao, Y. Sun, U. Coskun, FLIM Analysis using the Phasor Plots [Online]. Available, http://www.iss.com/resources/reference/data_tables/FL_LifetimeStandards.html.
[33] M.A. Digman, V.R. Caiolfa, M. Zamai, E. Gratton, The phasor approach to fluorescence lifetime imaging analysis, Biophys. J. 94 (2) (2008 Jan), https://doi.org/10.1529/biophysj.107.120154.
[34] F. Di Giacinto, C. Serantoni, M. De Spirito, G. Maulucci, Less can be more: optimization of the acquisition range to enhance phasor analysis in fluorescence lifetime imaging microscopy, Microsc. Microanal. 31 (2) (2025 Apr), https://doi.org/10.1093/mam/ozaf014.
[35] C. Stringari, Label-free separation of human embryonic stem cells and their differentiating progenies by phasor fluorescence lifetime microscopy, J. Biomed. Opt. 17 (4) (2012 Apr) 046012, https://doi.org/10.1117/1.jbo.17.4.046012.
[36] K. Blinova, et al., Mitochondrial NADH fluorescence is enhanced by complex I binding, Biochemistry 47 (36) (2008 Sep) 9636–9645, https://doi.org/10.1021/bi800307y.
[37] S.H. Hassanpour, A. Doroudi, Review of the antioxidant potential of flavonoids as a subgroup of polyphenols and partial substitute for synthetic antioxidants, Avicenna J. Phytomed. (2023 Jan 01), https://doi.org/10.22038/AJP.2023.21774. Mashhad University of Medical Sciences.